J. Synchrotron Rad. (1999). **6**, 6–18

A multiple-CCD X-ray detector and its basic characterization

Masayo Suzuki,[a]* Masaki Yamamoto,[b] Takashi Kumasaka,[b] Kazumichi Sato,[b] Hidenori Toyokawa,[a] Ian F. Aries,[c] Paul A. Jerram,[c] Daniel Gullick[c] and Tatzuo Ueki[b]†

[a]Japan Synchrotron Radiation Research Institute (JASRI), SPring-8, Mihara, Mikazuki-cho, Sayo-gun, Hyogo 679-5198, Japan, [b]The Institute of Physical and Chemical Research (RIKEN), Mihara, Mikazuki-cho, Sayo-gun, Hyogo 679-5143, Japan, and [c]EEV, Waterhouse Lane, Chelmsford, Essex CM1 2QU, UK. E-mail: msyszk@sp8sun.spring8.or.jp

(*Received 28 July 1998; accepted 2 November 1998*)

The Station Equipment Group of JASRI and the SR Structural Biology Research Group of RIKEN have designed and constructed a 4 × 4 array of CCD X-ray detectors called the 'multiple charge-coupled-device X-ray detector (MCCDX)' in collaboration with EEV in the UK. The novel features of the system are the lower demagnification factor of its fibre-optics taper assembly and the higher operational temperature, when compared with similar detector systems already in existence. The present paper describes the design concepts of the MCCDX system as well as the basic characterization of the constructed MCCDX system, which was carried out by using a conventional X-ray generator system prior to its installation on RIKEN beamline I (BL45XU) of the SPring-8 facility.

Keywords: X-ray detectors; area detectors; charge-coupled devices; SPring-8; protein crystallography.

1. Introduction

The SR Structural Biology Research Group of the Institute of Physical and Chemical Research (RIKEN) has been constructing an X-ray beamline, called RIKEN beamline I (BL45XU), at the SPring-8 facility in Japan (Yamamoto *et al.*, 1997). One of its major scientific missions is to carry out advanced protein crystallography employing the multiple-wavelength anomalous diffraction method (MAD). For this method it is essential to record diffraction data using at least three different wavelengths to minimize any possible systematic errors. To meet these requirements the beamline has been instrumented with a dichromatic undulator and a so-called 'trichromator', enabling the beamline to successively irradiate a crystal under study with three different wavelengths of highly brilliant X-rays in the energy range from 7 keV to 14 keV, without changing any other associated instrumental parameters. Since such a trichromatic X-ray diffraction image should be recorded, for example, at every 1° within 180°, oscillating a crystal with an oscillation range of 1°, a complete image data set will certainly be of the order of Gbytes. Therefore, one of the most important issues is to have a fast-readout two-dimensional X-ray detector in order that the experiment can proceed in the most efficient manner. In this respect, an X-ray area detector based on charge-coupled devices (CCDs) has been regarded as a highly suitable instrument in view of engineering today.

Since the 1980s there have been a number of projects conducted worldwide in order to realize CCD-based X-ray area detectors, and there are presently several types of CCD detectors commercially available (Deckman & Gruner, 1986; Strauss *et al.*, 1990; Eikenberry *et al.*, 1991; O'Mara *et al.*, 1992; Stanton *et al.*, 1992*a*,*b*, 1993; Gruner *et al.*, 1993; Phillips *et al.*, 1993; Stanton, 1993; Stanton & Phillips, 1993; Allinson, 1994; Castelli *et al.*, 1994; Naday, Ross *et al.*, 1994; Naday, Westbrook *et al.*, 1994; Tate *et al.*, 1995; Moy, 1996; Westbrook & Naday, 1997). Because the readout time of CCD-based X-ray area detectors can be significantly shorter compared with conventional image-plate systems, they become indispensable instruments for X-ray beamlines in synchrotron radiation facilities, especially in protein crystallography. They guarantee the high precision that is required in determining the positions and the intensities of the diffracted X-rays as well as fast readout times for minimizing the duty cycle.

Based on this prospective understanding, the Station Equipment Group of JASRI and the SR Structural Biology Research Group of RIKEN have designed and constructed a 4 × 4 array CCD X-ray detector in collaboration with EEV in the UK. The completed detector system is called the 'multiple charge-coupled-device X-ray detector system', referred to as the MCCDX system in this paper,

† Present address: Japan Synchrotron Radiation Research Institute (JASRI), SPring-8, Mihara, Mikazuki-cho, Sayo-gun, Hyogo 679-5198, Japan.

realizing one of the largest systems ever integrated among existing CCD-based X-ray detectors. The novel features of the system are the lower demagnification factor of its fibre-optics taper assembly of 2.2, and its higher operational temperature of 273 K, when compared with similar detector systems already in existence. Prior to installation on the beamline, the MCCDX system was investigated with a conventional X-ray generator system to characterize its detector parameters, such as the image distortion, spatial resolution, non-uniformity of its X-ray sensitivity and dynamic range in its X-ray intensity measurement. Together with its design concept, the present paper describes the MCCDX system and reports preliminary results obtained on these fundamental characteristics in the initial off-beamline test.

2. Design and construction of the MCCDX system

2.1. *General features*

For protein crystallography, especially routine diffraction experiments performed using synchrotron radiation sources, the requirements applied to two-dimensional detectors have been well specified (Helliwell, 1992; Allinson, 1994; Moy, 1996), along which the MCCDX system was also conceptually designed and constructed with some optimizations to RIKEN beamline I (BL45XU).

Fig. 1 shows the air- and light-tight aluminium vessel of the MCCDX system, which contains a 4 × 4 array structure of fibre-optic tapers (FOTs) as illustrated in Fig. 2. The large ends of the FOT assembly, functioning as the input ends, are coated with a scintillating screen, and the small ends, functioning as the output ends, are coupled to large formatted scientific CCDs with independent readout electronics. One may regard each element of the array structure as an independent CCD X-ray detector module to a certain extent. Since the scintillating screen, the FOT assembly and the CCDs were considered to be subject to further investigations and/or to replacements due to possible damage, they were designed to be replaceable as described in the following sections.

A flow of chilled ethylene glycol–water mixture is supplied to the vessel in order to regulate the operational temperature of the CCDs to be 273 K, of which the stability over 1 h and 24 h was measured to be within 0.05 K and 0.5 K, respectively. Nitrogen gas is also supplied to the vessel during the operation with a flow rate of 200 cc min^{-1} at 1.2 atm to avoid moisture condensation on the CCD packages and the mounted electronics. Table 1 summarizes the relevant parameters of the system, which are described below in detail.

2.2. *X-ray entrance window and detection area*

As shown in Fig. 1, the MCCDX system is equipped with an X-ray entrance window made of carbon-coated black mylar of thickness 150 µm and a 250 mm × 250 mm open area. The X-ray transmission of the window, T_w, is estimated to be T_w = 95% at 12.4 keV. Inside the vessel there exists a nitrogen layer of thickness 5 mm between the window and the FOT assembly for thermal isolation.

Among the many associated detector parameters, the extension of the active detection area that the FOT assembly possesses, H, is one of the most fundamental quantities because it ultimately limits the maximum resolution, d, of a protein crystal under study, which can be expressed by

$$d = \lambda_{\mathrm{X-ray}} / \sin[\arctan(H/2L)], \qquad (1)$$

where $\lambda_{\mathrm{X\text{-}ray}}$ denotes the wavelength of the incident X-ray and L is the camera length. With $\lambda_{\mathrm{X\text{-}ray}}$ = 1.0 Å, H = 200 mm and L = 200 mm, for example, the MCCDX system could attain d = 2.2 Å, which should be sufficiently high for standard protein crystallography. The value of d could be

Figure 1
Photograph of the multiple charge-coupled-device X-ray detector (MCCDX).

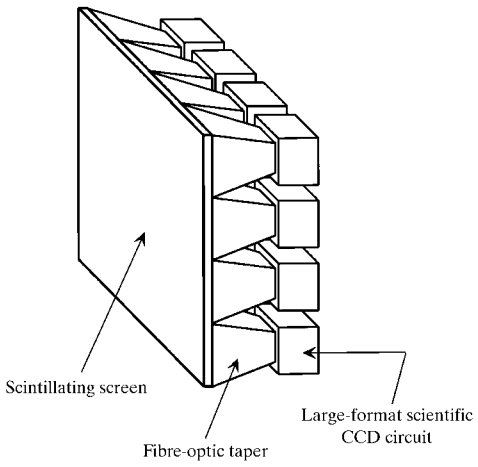

Figure 2
Schematic of the 4 × 4 array structure of the fibre-optic tapers coupled to the CCDs.

Table 1
MCCDX detector parameters.

Detector parameters	Designed value; measured value
General	
Energy range of incident X-ray photons	7–14 keV
Maximum resolution	2.2 Å @ 12.4 keV with 200 mm camera length
Minimum X-ray sensitivity	7 X-ray photons @ 12.4 keV with 1 s integration time
Horizontal and vertical spatial resolutions	50 μm × 50 μm (r.m.s.); <70 μm × 80 μm (r.m.s.)
Maximum detective quantum efficiency	0.76 @ 12.4 keV with 1 s integration time
CCD-limited dynamic range	7.7×10^3; 5.3×10^3–1.5×10^4
X-ray window	
Active area	200 mm × 200 mm
Material	Carbon-coated black mylar
Thickness	150 μm
Absorption	95% @ 12.4 keV
Scintillating screen	
Material	Gd_2O_2S(Eu)
Thickness	20 μm (10 mg cm^{-2})
Grain size	4 μm
Absorption	74% @ 12.4 keV
Fibre-optic taper matrix	
Matrix	4 × 4
Input end	50 mm × 50 mm
Output end	25 mm × 25 mm
Linear demagnification factor	2.0; 2.2
Charge-coupled device	
Model	CCD05-30/EEV
Image area	27.95 mm × 25.92 mm
Pixel format	1242 × 1152 pixels
Pixel pitch	22.5 μm × 22.5 μm
Quantum efficiency	42% @ 620 nm
Operational temperature	273 K
Operational mode	MPP
Full-well capacity	2.0×10^5 electrons pixel^{-1} in MPP mode
Dark noise	5.6 electrons pixel^{-1} s$^{-1/2}$ @ 273 K
Response non-uniformity	±3% of mean
Dark-noise non-uniformity	±2% of mean
Overall charge sensitivity	2.0 μV electron^{-1} @ 1 MHz
Readout noise	25 electrons pixel^{-1} @ 1 MHz
Readout time	~1.43 s @ MHz
Data acquisition system	
Number of ADCs	16
ADC resolution	16 bits
Conversion frequency	1 MHz
Conversion time	~1.43 s image^{-1}
Overall data size	43.5 Mbytes image^{-1}

further improved up to 1.8 Å, if needed, by shortening the wavelength of the X-ray beam to 0.8 Å, which is the shortest wavelength attainable at RIKEN beamline I, or simply by decreasing L at the expense of worsening the maximum interplanar distance detectable. Hence, the active detection area of 200 mm × 200 mm was considered to be an appropriate design value for the MCCDX system.

2.3. *Scintillating screen*

As Fig. 2 illustrates, the active detection area is covered with a layer of a scintillating phosphor where the incident X-ray photons are converted to visible scintillation photons. Gd_2O_2S-based phosphors were regarded as the primary candidate for the MCCDX system because they had been intensively investigated as promising substances, in particular Gd_2O_2S(Tb) (Chappell & Murray, 1984; Eikenberry *et al.*, 1991; O'Mara *et al.*, 1992; Gruner *et al.*, 1993; Moy *et al.*, 1993; Koch, 1994; Shepherd *et al.*, 1997). It has been reported that the light output from a Gd_2O_2S(Tb) phosphor under irradiation from 8 keV X-rays is maximized with a phosphor thickness of ~10 mg cm^{-2} (O'Mara *et al.*, 1992), with which the screen could absorb 97% of 8.1 keV X-rays and 66% of 13.6 keV X-rays (Gruner *et al.*, 1993). With reference to these works, a phosphor thickness of 10 mg cm^{-2} was adopted as a target value for the MCCDX system, with which 74% of 12.4 keV X-ray photons would be absorbed.

The scintillation characteristics of Gd_2O_2S-based phosphors are, however, known to be strongly dependent on the activators doped. For example, the maximum emission is observed around 540 nm in Gd_2O_2S(Tb), while that in Gd_2O_2S(Eu) is observed around 620 nm (Moy *et al.*, 1993; Shepherd *et al.*, 1997). Because the transmission of FOTs approaches the maximum value theoretically predicted in the wavelength region from 650 nm to 750 nm (Coleman, 1985) and the quantum efficiency of the particular model of the CCDs used for the MCCDX system has its maximum around 700 nm (EEV, 1994*a*), a scintillating screen based on Gd_2O_2S(Eu) was considered to be better suited to the present system when compared with the Tb-activated one.

One of the technical concerns of using a Gd_2O_2S(Eu) scintillating screen is, however, its time response to X-ray irradiation. Its decay time is reported to be about 4 ms for the relative intensity to decay to 10%, about 60 ms to decay to 1%, and 1 s to decay to 0.1% (Shepherd *et al.*, 1997), and it is known that the time response is highly dependent on the duration of X-ray irradiation (Flynt, 1989). In order for the MCCDX system to minimize the possible errors introduced by this rather long persistence of Gd_2O_2S(Eu), the system should be kept active for a few seconds even after terminating the X-ray irradiation, during which the afterglow component can be integrated appropriately.

In addition, it seems important not to reduce the temperature of the scintillating material far below 273 K, since scintillation decay constants are, in general, increased with decreasing temperature, although few studies have been reported on the temperature-dependence of Gd_2O_2S-based phosphors. Owing to its operational temperature of 273 K, the MCCDX system should be relatively free from this possible enhancement of the persistence under cryogenic conditions.

A reflective layer made of an aluminized mylar can be attached to a scintillating screen to increase the number of scintillation photons collected in the FOTs. It has been pointed out, however, that such a reflecting layer can not only absorb the incident X-ray photons but can also deteriorate the spatial resolution (Westbrook & Naday, 1997). It was therefore decided not to attach any reflecting layer to the present screen structure.

To fabricate a scintillating screen for the MCCDX system with the viewpoint discussed above, a thin layer of

Gd_2O_2S(Eu) (Nichia Chemical Industry, Tokyo) mixed into a plastic binder material with a thickness and a grain size of 20 μm and 4.0 μm, respectively, was first deposited on a Melinex polyester film of thickness 10 μm that was sprung onto a holding jig. The film, coated with a thin layer of Gd_2O_2S(Eu), was then transferred to the input ends of the FOT assembly, where the scintillating compound was solidified by warming up the assembly. Since the scintillating screen itself was considered to be subject to further investigation and possible damages, it was essential to adopt the film transfer method by which replacement of a scintillating screen can be accomplished on demand.

It is worth mentioning at this point that the number of scintillating photons, n_{ph}, emitted from the scintillating screen having an effective thickness of 10 mg cm^{-2} can be estimated to be $n_{ph} \simeq 400$ when an X-ray photon with an energy of 12.4 keV impinges on the screen (Moy *et al.*, 1993; Koch, 1994). Only half of them would be collected in the FOT because there is no reflecting layer employed on the present scintillating screen, as mentioned above.

2.4. *Fibre-optic tapers (FOTs)*

The luminous image induced by incident X-ray photons on the scintillating screen will be viewed with the FOT assembly as illustrated in Fig. 2, which reduces the image size so that it is entirely covered by the sensing areas of the CCDs attached to the output ends of the assembly. As discussed by Coleman (1985), the demagnification factor, D, of the FOTs plays the central role among the many parameters to be simultaneously optimized in designing them. As the value of D increases, the number of scintillation photons reaching the CCDs is reduced by a factor of D^2, and the image distortion will be enhanced as well, so it is recommended to utilize FOTs with $D < 3$ (Coleman, 1985). In order to suppress the image distortion near the edges of the FOTs to below 5%, at which level the image distortions introduced could be accurately corrected with appropriate software, the MCCDX system adopted $D = 2$ as its design value, which corresponds to an area reduction ratio of 25%.

The survey made on large formatted scientific CCDs commercially available at the time of designing the MCCDX system clearly indicated that a particular model of CCDs produced by EEV, *i.e.* CCD05-30, could meet almost all of the technical demands required by the MCCDX system. The reliability of the model had also been well confirmed by the satisfactory results reported not only in scientific applications but in industrial activities as well (Ashton, 1993). Given the fact that the sensing area of CCD05-30 is 27.95 mm × 25.95 mm, it was concluded that the matrix structure of the FOT assembly coupled to the CCDs should be 4 × 4, in order to cover the MCCDX active area of 200 mm × 200 mm entirely with $D = 2$. In terms of its dimensions, this implied that each FOT to be assembled should have input and output square ends of 50 mm × 50 mm and 25 mm × 25 mm, respectively.

It is well known that the amount of fibre defects contained in an FOT dictates its optical quality. In order to avoid the possible defects, Coleman's criterion suggests that the length of the FOTs should be larger than the diagonals of the input square ends by a factor of at least 1.5 (Coleman, 1985), which would correspond to 70 mm for the present case. Instead, the length of the FOTs for the MCCDX system was designed to be 50 mm, but applying to them such specification that the defect area, if any, should not exceed 50 μm × 50 μm per 1 mm × 1 mm on the input end of the FOT on average. The fibre size was designed to be 10 μm at the input ends in order to avoid excessive light losses, and extramural absorbers were included for controlling the propagation of stray light.

If the MCCDX system were to be operated at a temperature far below 273 K, assembling the 4 × 4 matrix structure of these FOTs should have been technically much more difficult, because thermal contraction could seriously loosen the mutual contacts among the FOTs irrespective of the mechanism employed to combine them as a single body. From the viewpoint of the CCD noise performance as discussed below, however, the operational temperature was decided to be 273 K, at which temperature such a method could still be stable and reliable that all FOTs are combined by mechanical compression with a stainless-steel frame as shown in Fig. 3. In this method, a dead space for adjacent FOTs of 100 μm is certainly attainable, and possibly as good as 50 μm, because it should be mostly controlled by the mechanical tolerance of the FOTs when no adhesive is used. In fact, these prospective values were confirmed by the dead-space measurements as reported in §2.6. It was important for the MCCDX system to adopt the mechanical compression method since it would provide the system with

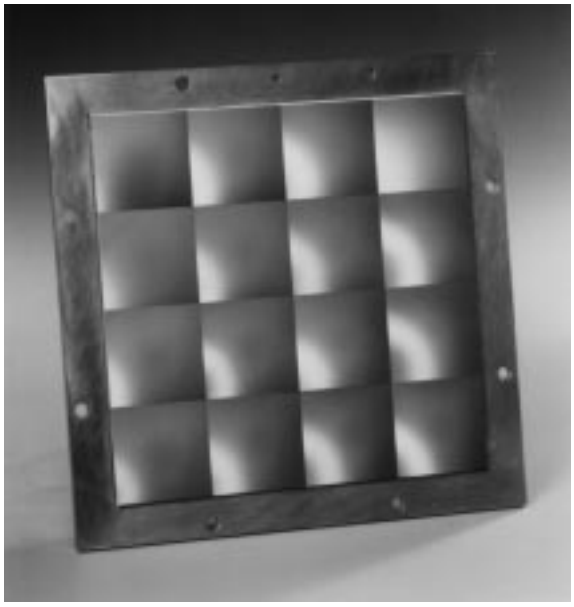

Figure 3
Photograph of the stainless-steel frame combining all the FOTs under mechanical compression.

the flexibility to replace any of the FOTs, if needed, without damaging the rest of the structure.

It should be noted here that, after being transmitted through the FOTs as described above, the number of scintillation photons reaching the output ends of the FOTs, $n_{\rm FOT}$, should be reduced to $n_{\rm FOT} \simeq 50$ due to the demagnification process.

2.5. *CCDs*

As already specified, the model of the CCDs adopted for the MCCDX system is CCD05-30, which is one of the large formatted scientific CCDs produced by EEV, UK. The model has an image area of 27.95 mm × 25.92 mm with a pixel format of 1242 × 1152, having a pixel size of 22.5 μm × 22.5 μm. It has a spectral response in the wavelength region from 420 nm to 1100 nm with a maximum quantum efficiency of 47% at 700 nm. When operated in MPP mode with an operational temperature of 273 K (see §2.7), the model typically indicates a dark noise and a full-well capacity of 6 electrons pixel^{-1} s^{-1} and 2.0 × 10^5 electrons pixel^{-1}, respectively. Its non-uniformities in response and in dark noise over the pixels are usually ±3% of the mean and ±2% of the mean, respectively.

An appropriate coupling method has to be employed to attach the CCDs to the output ends of the FOT assembly in order to minimize the possible light loss and/or image degradation at their boundaries. Coating a thin layer of optical gel with a precisely adjusted optical index between the CCD window material and output ends of the FOT assembly under mechanical compression would serve as the best joint in this respect. In addition, this method allows the mounted CCDs to be detached from the assembly in a relatively easy way, thus enabling the CCDs to be replaced by new ones, not only for maintenance but also for future improvement. The operational temperature of the system of 273 K could again be in favour of adopting this method because the gel would not be seriously hardened at this temperature.

Based on the design concept of RIKEN beamline I, it is assumed in the following discussion that the X-ray beam under consideration has a beam size of 100 μm × 100 μm. If, therefore, the scintillating screen has a point spread function well represented by a Gaussian function with a standard deviation of 100 μm, the optical images of the diffraction spots could be 140 μm in diameter on the scintillating screen, and would be reduced to 70 μm in diameter at the output ends of the FOTs. Since the CCDs adopted have a pixel size of 22.5 μm × 22.5 μm, the major part of the diffraction spots would be viewed by a local pixel matrix of 3 × 3 on average. Unless the luminescence intensity of the spot is comparable with the noise level of the system, sampling a diffraction spot with a 3 × 3 pixel matrix should, in principle, result in providing enough information to determine not only the intensity of the X-ray spot as precise as the system DQE predicts, but also the locations of the spots on the scintillating screen within the horizontal and vertical spatial resolutions of the present system, σ_x and σ_z.

Given that the quantum efficiency of the CCDs reaches 42% at a wavelength of 620 nm (EEV, 1994*a*), one can estimate the total number of photoelectrons, $N_{\rm el}$, induced by a 12.4 keV X-ray photon in the corresponding 3 × 3 local pixel matrix to be $N_{\rm el} \simeq 20$ electrons, assuming that the optical transmission is very close to unity at the boundaries where the output ends of the FOTs are interfaced with the CCDs with the gel coupling method described above. Among the local pixels observing the scintillation spot caused by a single incident 12.4 keV X-ray photon, the number of photoelectrons generated in the central pixel, $n_{\rm el}$, could be $n_{\rm el} \simeq 5$ on average.

2.6. *Examination of the completed FOT–CCD assembly*

Following the design concepts presented above, a 4 × 4 FOT assembly was completed at Shott Fiber Optics, USA, and then 16 chips of model CCD05-30 were attached to the FOT assembly at EEV, UK. Before attaching them, it was confirmed that all CCD chips to be used had a dark-signal non-uniformity within ±3% of the mean and a photoresponse non-uniformity within ±2% of the mean. The completed FOT–CCD assembly was then subjected to various measurements under white-light illumination such as (i) image distortion, (ii) spatial resolution, (iii) dead space, (iv) cross-talk and (v) CCD-limited dynamic range, prior to the scintillating screen transfer process.

In order to evaluate the image distortion, the linear demagnification factors at the centre, D_C, and near the edge, D_E, of each FOT were measured with an optical test pattern. The measured values of D_C and D_E averaged over 16 FOTs were 2.18 and 2.24, respectively, which were about 20% higher than the designed value. With the definition of the measure of image distortion, Δ, as

$$\Delta(\%) = (D_C - D_E)/D_C \times 100, \qquad (2)$$

the numerical values of Δ calculated from the measurements were all less than 3% for the completed FOT–CCD assembly.

The spatial resolution of the assembly was evaluated by recording the edge functions of a sharp black-to-white transition placed vertically and horizontally on the input ends of the assembly. The edge functions observed for the 16 FOT–CCD modules fell to 16% of the peak signal within one pixel, 9% within two pixels and 6% within three pixels on average.

By defining the dead space, $d_{\rm dead}$, as the local area at the vicinity of the FOT boundary where the light intensity decreases to less than 50% of that in other regions, the values of $d_{\rm dead}$ were evaluated by placing a test chart containing a V-shape pattern in front of the input ends of the FOT assembly. The observed values of $d_{\rm dead}$ were around 50 μm on average, and less than 100 μm in the worst case.

In order to evaluate the cross-talk among the 16 CCD modules, a small square area in a CCD was illuminated at a

level close to saturation and the output from adjacent CCDs was measured. It was concluded from the measurements that the cross-talk was suppressed below a level of 1/8000 among all CCD modules.

Under the MPP mode operation (see §2.7), the CCD-limited dynamic ranges of the 16 CCD modules were evaluated by dividing the observed maximum output from the modules by the observed standard deviation of noise at a readout frequency of 1 MHz with an operational temperature of 273 K, and were found to vary module by module from 5.3×10^3 up to 1.5×10^4, yet being in agreement with the theoretical evaluation given in §2.7.

These examinations, made prior to the scintillating screen transfer process, verified that the completed FOT assembly had functioned as designed under white-light illumination. If, therefore, any of these measured detector parameters became worse after transferring the screen to the FOT assembly, one could easily attribute them to the scintillating screen.

2.7. *Noise estimation in the CCDs and their readout circuits*

Thermal generation of electrons in CCDs is the mechanism responsible for their dark signal, which is one of the major limiting factors of noise performance in a given CCD-based system along with the readout noise. At an operational temperature of 273 K, a CCD05-30 would indicate a dark signal of $n_{\rm dark} \simeq 3.2 \times 10^3$ electrons pixel^{-1} s^{-1} with a statistical fluctuation of $\sigma_{\rm dark} \simeq 56$ electrons pixel^{-1} s$^{-1/2}$ (r.m.s.). Cooling the CCDs is definitely an effective way of reducing the dark signal. In fact, the dark signal could be decreased by about two orders of magnitude by reducing the operational temperature from 273 K to 228 K, although it is anticipated that assembling the 4×4 FOT matrix structure could be technically difficult because of thermal contraction, as already mentioned.

Another way of reducing the dark signal is to operate CCDs in the multi-pinned phase, usually referred to as MPP mode, by which the thermal generation of electrons in CCDs is highly suppressed by the presence of intentionally located holes (Ashton, 1993). At an operational temperature of 273 K, a CCD05-30 under MPP-mode operation could indicate a dark signal of $n_{\rm dark} \simeq 32$ electrons pixel^{-1} s^{-1} with a fluctuation of $\sigma_{\rm dark} \simeq 5.6$ electrons pixel^{-1} s$^{-1/2}$ (r.m.s.), which is two orders of magnitude better than the normal-mode operation under the same operational conditions, and is significantly less than the readout noise at a readout frequency of 1 MHz, as given below. This implies that there is no necessity to reduce the CCD operational temperature further under the given conditions.

Along with the dark signal generated in the CCDs themselves, it is well known that the readout noise, $\sigma_{\rm readout}$, is another determinant of the overall noise performances of CCD-based instruments; the readout noise is the electronic noise in the CCD readout circuit, mainly caused by resetting the CCD output nodes and by operating the output transistor in the MHz frequency region. The reset noise, however, can be effectively eliminated by sampling the output waveform twice, once after resetting and again after charge output, and by taking the difference between the successive waveforms sampled, which is called the 'correlated double-sampling technique'. This sampling technique also effectively reduces the output transistor noise with an appropriate sampling interval, $\tau_{\rm sampling}$, because it can function as a band-pass filter at the optimal region. In fact, by using the correlated double-sampling technique with $\tau = 10$ µs, the readout noise of a CCD05-30 can be as low as $\sigma_{\rm readout} \simeq 25$ electrons pixel^{-1} (r.m.s.) at a readout frequency of 1 MHz.

Since the overall noise of the MCCDX, $\sigma_{\rm overall}$, is written as

$$\sigma_{\rm overall} = (\tau_{\rm int}\sigma_{\rm dark}^2 + \sigma_{\rm readout}^2)^{1/2}, \qquad (3)$$

$\sigma_{\rm overall}$ in the present system can be numerically evaluated as $\sigma_{\rm overall} = (31.3\tau_{\rm int} + 625)^{1/2}$, where $\tau_{\rm int}$ denotes the integration time of the CCDs. Fig. 4 displays $\sigma_{\rm overall}$ as a function of $\tau_{\rm int}$ together with the full-well capacity of the CCD in MPP mode. Based on the estimation made above, the overall noise level of the MCCDX can be evaluated to be $\sigma_{\rm overall} \simeq 26$ electrons pixel^{-1} (r.m.s.) with $\tau_{\rm int} = 1$ s at a readout frequency of 1 MHz. Recalling that a 12.4 keV X-ray photon would yield about five photoelectrons in a central pixel of the CCDs, one could infer that, in order for the signal level to exceed the overall noise, (S/N) > 1.0, more than seven X-ray photons of this energy should impinge on the same location of the scintillating screen through the entrance window while the system continues its charge integration process for 1 s under operational temperature and readout frequency of 273 K and 1 MHz, respectively. In other words, the minimum X-ray peak sensitivity, $s_{\rm min}$, of the MCCDX system could be $s_{\rm min} \simeq 7$ X-ray photons at 12.4 keV under the present conditions.

The overall noise performance also limits the range of signals that can be measured with the MCCDX system, *i.e.* the dynamic range, DR, which is defined as

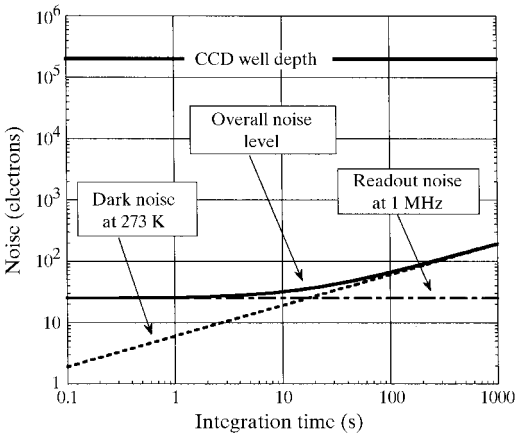

Figure 4
Overall noise level expected in the MCCDX as a function of integration time.

$$\mathrm{DR} = (N_{\max}/\sigma_{\mathrm{overall}}), \quad (4)$$

where $N_{\max}$ denotes the maximum number of electrons stored in a single pixel of a CCD, *i.e.* the full-well capacity. The value of $N_{\max}$ reaches 2.0×10^5 in a CCD05-30 in MPP mode, so that DR could be 7.7×10^3 in the present case. The maximum X-ray peak measurable in the MCCDX system, $S_{\max}$, determined in the dynamic range would be $S_{\max} \simeq 5.5 \times 10^4$ X-ray photons at 12.4 keV for an integration time of 1 s.

One may be concerned with external noise sources such as cosmic rays. The dominant portion of the hard component in cosmic rays at sea level is known to be muons in the minimum ionization region, which have an energy loss of $(\mathrm{d}E/\mathrm{d}x)_{\min} \simeq 1$ MeV cm^2 g^{-1} with an approximate event rate of 1 muon m^{-3} s^{-1} (Particle Data Group, 1994). Vertically passing through the FOT assembly with an effective density of 2.6 g cm^{-3}, a minimum ionizing muon could leave an energy of 50 MeV in the FOTs along its path of 20 cm, or 11 keV per 45 µm, which would be viewed by a single pixel of the CCD. Assuming that the FOTs have an absolute scintillation efficiency, ε, as high as that of Li glass, *i.e.* ε = 1.5% (Knoll, 1989), and the maximum emission appears at 395 nm at which the quantum efficiency of the CCD becomes less than 5% (EEV, 1994*a*), the number of photoelectrons generated in the CCD pixel can be estimated to be less than 3 electrons pixel^{-1}, being too faint to be detected with the present system.

Passing through a CCD directly, on the other hand, a minimum ionizing muon could leave 80 electron–hole pairs per mm in silicon. Since it corresponds to a generation of 2×10^3 electrons in a single pixel with a silicon thickness of 25 µm (EEV, 1987), the passage of minimum ionizing muons in any of the CCDs should be detectable in the present system. Such a cosmic muon passage in a CCD has been reported to have a rate of several events per minute, so that there is a good chance that an X-ray image acquired with the MCCDX system contains a peak caused by a cosmic muon with an integration time of 1 s (EEV, 1987). In practice, one could identify the arrival of muons by triggering the MCCDX system with a scintillation counter telescope, for example, but no such experiment has been attempted yet.

2.8. *Signal and data processing*

Those electrons created in a CCD, either by incident X-ray photons or by the thermal excitation process, will be detected and converted into a pulse with a charge-sensitive preamplifier associated with the CCD. With a charge sensitivity of 2.0 µV electron^{-1} of the preamplifier mounted on a CCD05-30, the minimum and maximum X-ray peaks detectable in the dynamic range of the present system would generate pulses with amplitudes of 0.05 mV and 400 mV, respectively. In order to digitize the pulses in this range, it is reasonable to have an A/D converter that can accept the input pulses ranging between 0 V and 1 V with a resolution of 16 bits, which corresponds to ~15 µV per A/D count. Under these conditions the minimum X-ray peaks detectable would correspond to 4 ± 2 counts in the A/D converters, disregarding the pedestal and the noise that the converters should have.

Because the 16 CCD X-ray detector modules of the MCCDX system will be operated at 1 MHz simultaneously, it is also clear that all of the 16 outputs from the system should be digitized in parallel with 16 independent A/D converters with a conversion frequency of 1 MHz in order to optimize the duty cycle of the system. There are 1430784 pixels in each CCD05-30, so that it would take slightly longer than 1.43 s for each A/D converter to digitize and locate the image data of 2.72 Mbytes in their buffer memories. Since there will be 16 digital images to be delivered to an associated computer, it would take 4.35 s for the system to complete its transfer process for these 16 digital images with a data transfer rate of 10 Mbytes s^{-1}. For locating the complete data set to a hard disk, it would take a further 6.2 s with a data transfer rate of 7 Mbytes s^{-1}. Assuming that the X-ray beam exposure time lasts 1 s followed by the persistence compensation time of another 1 s, the MCCDX system should be able to take an X-ray diffraction image every 14 s, which could be an appropriate duration for re-orienting the sample under investigation as well as for carrying out the initial data processing such as background subtraction, image distortion correction, non-uniformity correction and indexing. With this data-collecting cycle, it would take 42 min for RIKEN beamline I to acquire a complete set of X-ray diffraction images taken every 1° within 180°, reducing them to indexing tables. Since the size of the data file containing these indexing tables should be of the order of several Mbytes at maximum, one could attempt to send the file over local-area network to a main-frame computer, where structure analysis of the sample under study can be accomplished.

The readout electronics actually mounted on each CCD module of the MCCDX system are a variant of the CCD driver assembly (CDB01-X, EEV) that was able to comply with the geometrical constraints of the system (EEV, 1994*b*). These drivers can also accept an external trigger pulse, whose width defines the integration time of the system. Upon detecting the end of the trigger pulse, the driver assemblies start reading out the CCDs and process the charge signals based on the correlated double-sampling technique as mentioned previously. The data-acquisition system linked to the MCCDX consists of a digitizer (MCCDX I/F, System Design Service Corporation, Japan) and a workstation (DEC Alpha Station 600 5/266). The digitizer is a VME-based system equipped with 16 modules of ADCs. Upon receiving an external start-pulse synchronizing with the MCCDX operation, these ADC modules start digitizing all the MCCDX output signals simultaneously into digital signals of 16 bits with a sampling rate of 1 MHz. Each module has a buffer memory of 3 MB, and the stored data are transferred to the workstation *via* a VME/PCI interface for data storage and further analysis.

2.9. *Detective quantum efficiency*

The overall performance of the MCCDX system described so far can be foreseen by estimating the detective quantum efficiency, DQE, which is defined as

$$\mathrm{DQE} = (S_{\mathrm{out}}/\sigma_{\mathrm{out}})^2/(S_{\mathrm{in}}/\sigma_{\mathrm{in}})^2, \qquad (5)$$

where σ_{out} denotes the standard deviation of the output signal with a mean value of S_{out}, and σ_{in} denotes the standard deviation of the input signal with a mean value of S_{in}. Following the theoretical consideration given by Stanton *et al.* (1993), the predicted DQE of the present system as a function of the number of incident X-ray photons, I, can be expressed as

$$\mathrm{DQE}(I) = T_w/[1 + R_s + 1/G + S(\sigma^2_{\mathrm{readout}} + n_{\mathrm{dark}}\tau_{\mathrm{int}})/IT_wG^2], \qquad (6)$$

where T_w denotes the fraction of incident X-ray photons transmitted by the entrance window, R_s is the phosphor noise factor, G is the detector gain (number of photoelectrons per incident X-ray photon) and S is the peak integration area (pixels).

Among the various parameters included in the above equation, the values of T_w and R_s largely affect its asymptotic behaviour. As described previously, the MCCDX system has an X-ray entrance window made of mylar with a thickness of 150 µm and a nitrogen gas layer of 5 mm in front of the scintillating screen, to which an incident X-ray would have a transmission of T_w = 95% at 12.4 keV. Since R_s represents the effect of scattering and absorption processes of the scintillation photons in the scintillating screen, its value depends on the phosphor type, the grain size and deposition procedure, varying in the range from 0.0 to 0.2 (Stanton *et al.*, 1992). Using the most conservative value of R_s = 0.2 together with G = 20 photoelectrons per 12.4 keV X-ray photon, S = 9 pixels, $\sigma_{\mathrm{readout}}$ = 25 electrons pixel^{-1}, n_{dark} = 32 electrons pixel^{-1} s^{-1} and τ_{int} = 1.0 s as discussed above, the numerical value of the predicted DQE(I) can be written as DQE(I) = 0.95/(1.25 + 15.6/I) with incident X-ray photons of 12.4 keV in the present system, which asymptotically approaches its maximum value of 0.76 with increasing I, as shown in Fig. 5.

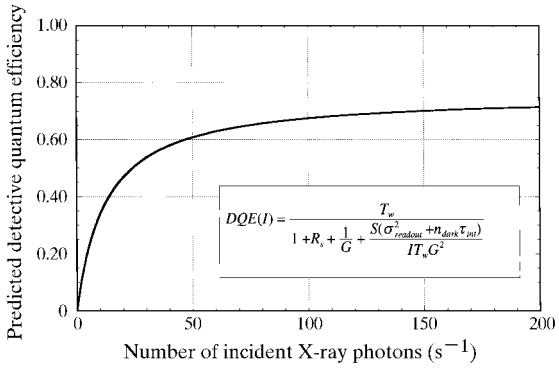

Figure 5
Predicted DQE as a function of the number of incident X-ray photons.

3. Experimental and discussion

3.1. *Experimental set-up*

Having confirmed that the MCCDX system responded to white-light illumination as designed, the scintillating screen was transferred to the FOT–CCD assembly in accordance with the method described in §2.3, and the basic performance of the system thus X-ray sensitized was evaluated by using a conventional X-ray generator system illustrated in Fig. 6. The X-ray generator used was a high-brilliance type with a fine-focus molybdenum rotating anode and was operated at 60 kV and 40 mA. The X-ray beam extracted from the generator was primarily shaped rectangularly with the first *XY* slits. A mechanical shutter was used to turn on and off the X-ray beam downstream under the control of a personal computer. The X-ray chopped beam was further collimated with an X-ray mirror, and then monochromated with an X-ray monochromator of a silicon triangular crystal at an X-ray wavelength of 0.7107 Å, focusing on the entrance window of the MCCDX through the second *XY* slits. The MCCDX itself was mounted on a precise *XZ* stage that was able to position the MCCDX with an accuracy of 50 µm in the vertical and horizontal directions.

3.2. *Image distortion*

With the *XZ* stage and the shutter operating synchronously, the MCCDX system was irradiated by the X-ray beam in such a way that the final image should result in the formation of a lattice pattern with horizontal and vertical intervals of 2 mm. Fig. 7 shows a typical example of the lattice images for a single CCD X-ray detector module. As expected, the resultant image indicates that there exists a pin-cushion-type image distortion.

During the course of evaluating a CCD-based X-ray detector, it is essential to employ software that can precisely examine and effectively correct the distorted images. In the present work, the software known as *FIT2D*, developed by A. P. Hammersly *et al.* at the ESRF, was adopted since it is one of the most advanced pieces of software available in this area (Hammersley *et al.*, 1994, 1995, 1997). By using *FIT2D*, the horizontal and vertical

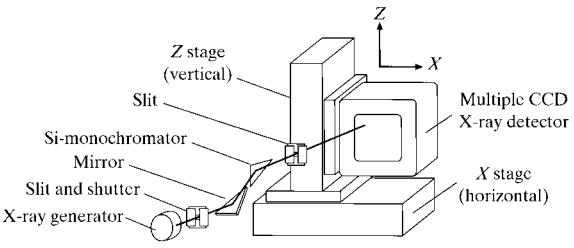

Figure 6
Schematic of the X-ray generator system used to evaluate the basic performance of the MCCDX.

Table 2
Horizontal and vertical average pixel sizes evaluated using *FIT2D*.

	Average pixel size (μm)															
Module number	01	02	03	04	05	06	07	08	09	10	11	12	13	14	15	16
Horizontal	49.21	49.67	49.83	49.66	49.66	49.33	49.03	49.86	49.89	49.27	49.14	49.97	49.72	50.10	49.50	49.38
Vertical	49.27	49.59	49.56	50.07	49.62	48.95	49.54	49.98	49.94	49.54	49.78	49.77	49.88	49.83	49.92	49.40

deviations of the observed X-ray beam positions from the those defined with the precise XZ stage, $\delta x(x)$ and $\delta z(z)$, were numerically evaluated as a function of the x- and z-coordinate, and are displayed in Figs. 8(a) and 8(b), respectively. Although the values of δx and δz are both of the order of 0.1 mm, or even less at the central region of each FOT, they become as large as 2 mm near its edges. It was found that all the CCD X-ray modules indicate almost the same coordinate dependencies.

Since the pixel size projected onto the input end of the FOT is position-dependent due to the complicated pin-cushion-type distortion, it is not possible to characterize the distortion exactly with a single parameter. However, since *FIT2D* offers to calculate such single parameters as 'the average pixel size' projected onto the input end of the FOT, this could be a useful measure in practice. By comparing it with the pixel size optically determined, which is 49.5 μm in the present case, one could infer the significance of the distortion. Table 2 summarizes the average pixel sizes evaluated for all the CCD X-ray detector modules. Since the average pixel sizes are in good agreement with those values optically determined, one could conclude that the X-ray image distortion observed was as good as that evaluated with white-light illumination, *i.e.* better than 3%.

3.3. *Spatial resolution*

The lattice images described above can provide information not only on the image distortion but also on the spatial resolution. The X-ray peaks observed on the top left, top right, centre, bottom left and bottom right in each lattice image that the 16 CCD X-ray detector modules detected were first extracted from the lattice images and then fitted to a Gaussian distribution function to express their vertical and horizontal spreads in terms of the root mean square, *i.e.* σ_x and σ_z. It was found that neither σ_x nor σ_z indicated any strong module- or position-dependencies. The values of σ_x and σ_z averaged over the 16 modules were found to be 69.7 ± 5.5 μm and 79.9 ± 10.6 μm, respectively.

Assuming that the Gaussian distribution function truly represents the observed X-ray peak profile, $f_{\rm peak}$, one may evaluate the vertical and horizontal full widths at 10% maximum of $f_{\rm peak}$ to be 150 μm and 170 μm, as well as those at 1% maximum of $f_{\rm peak}$ to be 210 μm and 240 μm, respectively. Since, however, the sizes of the local pixel matrices that covered the X-ray peaks in the lattice image with sufficiently high signal-to-noise ratios were limited to

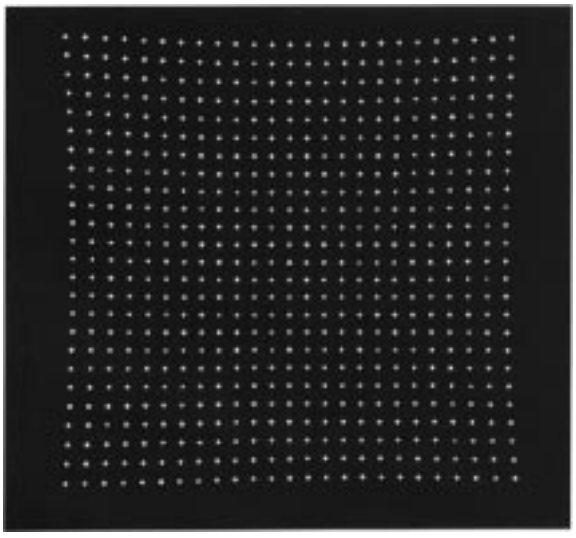

Figure 7
The lattice image observed with a single CCD X-ray detector module of the MCCDX.

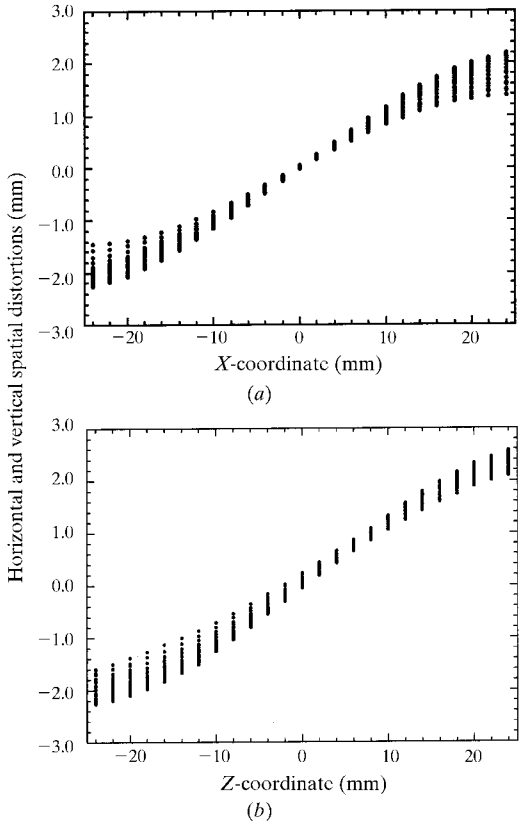

Figure 8
The distortions observed in (a) the horizontal direction and (b) the vertical direction on a single CCD X-ray detector module with reference to precisely defined X-ray beam spots.

below 5 × 5, it should be emphasized that the values estimated at the full width at 10% maxima could still be reliable, but those at the full width at 1% of the maxima become less reliable.

In addition, $f_{\rm peak}$ should not be regarded as the point spread function of the MCCDX system, $\mathrm{PSF_{MCCDX}}$, because the effect of the incident beam profile, $f_{\rm beam}$, upon $f_{\rm peak}$ has not been removed. To adequately evaluate $\mathrm{PSF_{MCCDX}}$, one should deconvolute $f_{\rm peak}$ with $f_{\rm beam}$. The deconvolution requires accurate measurements of $f_{\rm beam}$ by using, for example, a pin-hole scanning system, but reliable measurements have not been completed at the time of writing this paper. Nevertheless, it is conceivable that the inherent spatial resolution of the MCCDX is better than the present values of σ_x and σ_z cited above, since they were spatially smeared by the spread of the incident X-ray beam.

3.4. *Non-uniformity in X-ray sensitivity*

Evaluation of the non-uniformity in X-ray sensitivity of a two-dimensional X-ray detector, in general, requires a uniform field of X-rays wide enough to cover the entire region of the active detection area. Under the constraints of the present set-up, the practical method was to utilize the beam fan of the direct X-ray beam achieved by the elimination of all associated optical components. The MCCDX system was exposed for 8 s to the quasi-uniform field of X-rays thus generated. The image obtained with the central CCD X-ray detector module is displayed in Fig. 9(*a*) and its three-dimensional plot is displayed in Fig. 9(*b*). It can be clearly seen from Fig. 9(*b*) that the observed variation of the X-ray intensity is composed of a low-frequency component representing the global structure of X-ray sensitivity in the MCCDX system and a high-frequency component representing the associated local fluctuation.

By smoothing the global structure extracted from the original image over the two-dimensional 100 × 100 pixel range, it was found that the X-ray intensities observed at the edges are about 20% lower than those at the centres in this module. This global non-uniformity can mainly be attributed to the fact that the acceptance angles of the FOTs, within which light incident upon the input end of the FOTs can travel to the output ends, decrease as the incident location is moved from the centres to their edges. In order to perform a numerical analysis, the global structure was fitted to an empirical formula composed of a two-dimensional Gaussian distribution function and a linear function,

$$I(x,z) = I_0 \exp[-(x-x_0)^2/2\rho_x^2] \times \exp[-(z-z_0)^2/2\rho_z^2] + ax + bz + c, \quad (7)$$

where I_0 denotes the peak intensity, x_0 and ρ_x denote the peak position and its standard deviation in the x-coordinate, respectively, while z_0 and ρ_z denote those in the z-coordinate, respectively. The linear function has been included in the fitting function to correct the global inclination, potentially occurring in the x and/or z directions due to the minor misalignment of the MCCDX system with respect to the X-ray beam coming from the generator. In the case of Figs. 9(*a*) and 9(*b*), the best-fitted values estimated for those parameters appearing in (7) were I_0 = (1.916 ± 0.121) × 10^4 A/D counts, x_0 = (5.812 ± 0.129) × 10^2 pixels, ρ_x = (4.690 ± 0.243) × 10^2 pixels, z_0 = (5.808 ± 0.119) × 10^2 pixels, ρ_z = (4.591 ± 0.024) × 10^2 pixels, a = 0.558 ± 0.670 A/D counts pixel^{-1}, b = −1.467 ± 0.626 A/D counts pixel^{-1}, c = (3.454 ± 0.149) × 10^4 A/D counts pixel^{-1}, with which the reduced χ^2 value reached 3.89. Because the amplitude determined has an uncertainty of ∼5%, it should be pointed out here that any X-ray images of which non-uniformity has been corrected with this function are subject to the propagation of this uncertainty.

3.5. *Local fluctuation observed in X-ray intensity measurements*

It seems that the fitting uncertainty mainly originates from the local fluctuation in the image. The local fluctua-

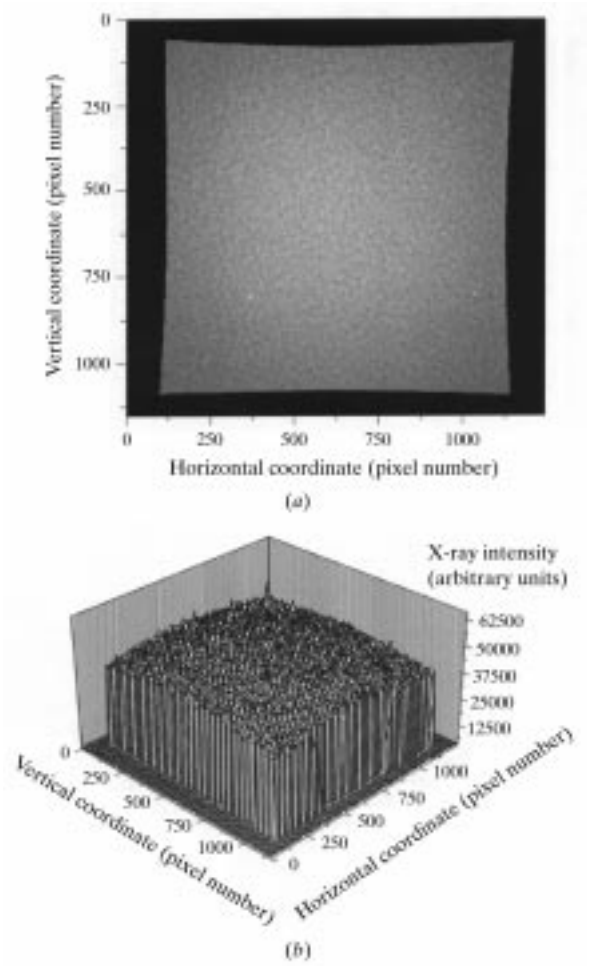

Figure 9
(*a*) The response image observed with a single CCD X-ray detector module to a quasi-uniform X-ray field. (*b*) The response image observed with a single CCD X-ray detector module to a quasi-uniform X-ray field represented by a three-dimensional plot.

tion can be obtained by subtracting the global structure determined from the original image, as shown in Fig. 10(*a*). The amplitude distribution of the fluctuation in the quasi-uniform field image is well represented by a Gaussian distribution, having a mean value of $I_{HF} = 33.5 \pm 3.8$ A/D counts and a standard deviation of $\sigma_{HF} = 1451 \pm 5$ A/D counts, as displayed in Fig. 10(*b*). The closeness of the mean value to zero indicates that the global structure subtraction process was adequately performed.

To reveal the nature of the local fluctuation, Fourier analysis can be one of the most effective methods. Fig. 11 shows the two-dimensional Fourier power spectrum of the fluctuation displayed in Fig. 10(*a*). As can be seen from Fig. 11, in addition to low-frequency components there are several distinctive peaks observed in the power spectrum at a particular spatial frequency of 150 cycles, as well as their harmonics. This implies that a certain structure with a physical dimension of ~300 μm was distributed over the local fluctuation structure, which almost corresponds to the size of the grain clusters occurring in the scintillating screen, as one may recognize in Fig. 9(*a*). This interpretation can be further supported by the fact that the distinctive peaks are time invariant and commonly observed in all Fourier power spectra of the 16 flat-field images. The temporal and spatial variations in the flat-field X-ray beam employed were certainly sources of further possible external noise, narrowing the dynamic range of the MCCDX system.

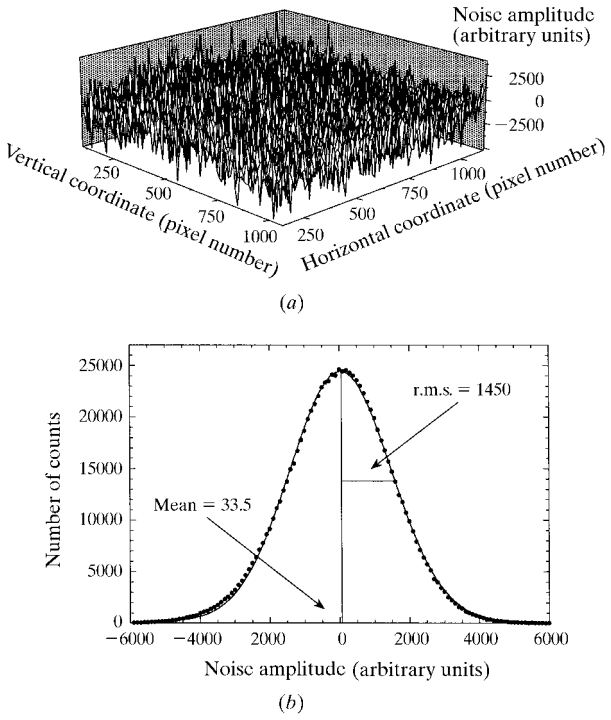

Figure 10
(*a*) The local noise component extracted from the quasi-uniform X-ray field image. (*b*) The amplitude distribution observed in the local noise component.

3.6. *Overall performance of the MCCDX system as an X-ray imager*

While evaluating the non-uniformity and the dynamic range of the MCCDX system, an X-ray transmission image of a twig with leaves was taken in order to examine the overall performance of the imaging system, as displayed in Fig. 12(*a*), in which the image distortion and the non-uniformity have both been corrected in accordance with the discussion above. Also displayed in Figs. 12(*b*) and 12(*c*) are the images magnified by a factor of 4 and 11.8, respectively. One can easily recognize the clearly resolved vein structure of the leaves with the MCCDX system.

It may be worth commenting on two independent methods of combining all 16 X-ray sub-images into a single unified X-ray image. The first method is practical, but only applicable when there is any continuous structure in the X-ray image across all boundaries of the FOT–CCD assembly. The unification in this case can be performed by joining all the sub-images in such a way that the structure in the unified image becomes continuous and smooth across all boundaries. The X-ray transmission image of the twig with leaves presented above was unified in this method with a butting inconsistency of a few pixel lines. In the second method, essentially all the pixels in the MCCDX system will be first calibrated about their locations in a single frame of x- and z-coordinates by using the lattice image taken with the precise XZ stage described previously, and all the sub-images are then combined with reference to their calibrated coordinates. Although the positioning accuracy of the stage ultimately limits the ambiguity of the unification process, this method is more precise than the first method and applicable to any X-ray images, even if there is no continuous structure contained, hence is better suited for such discrete images as X-ray diffraction patterns.

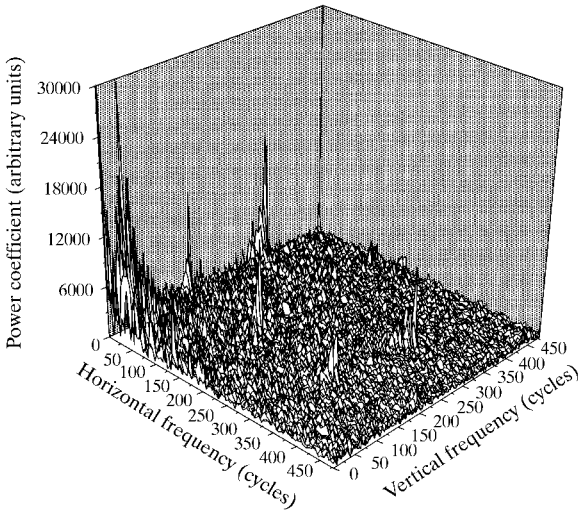

Figure 11
Two-dimensional Fourier power spectrum of the local fluctuation.

4. Concluding remarks

A 4 × 4 array of CCD X-ray detectors called the multiple charge-coupled-device X-ray detector (MCCDX) has been constructed with the novel features of a low demagnification factor of the fibre-optics taper assembly (D = 2.2) and a moderate operational temperature (T_{CCD} = 273 K). The system performance has been satisfactory confirmed in different aspects through an examination made on the FOT–CCD assembly during its integration process and through the basic characterization made on the complete system with a conventional X-ray generator system. One can, therefore, expect the MCCDX system to function as a significant part of RIKEN beamline I (BL45XU) at the SPring-8 facility, where research on advanced protein crystallography is being performed based on the trichromatic concept. Various tests are, however, waiting to be performed for the MCCDX system at the beamline to verify whether it is successfully installed, not only in terms of hardware but also in terms of software. To that end, the MCCDX system will be acquiring a vast amount of X-ray diffraction images of well known protein samples during the period of commissioning, through which the detector parameters will be re-examined under the irradiation of a synchrotron radiation X-ray beam.

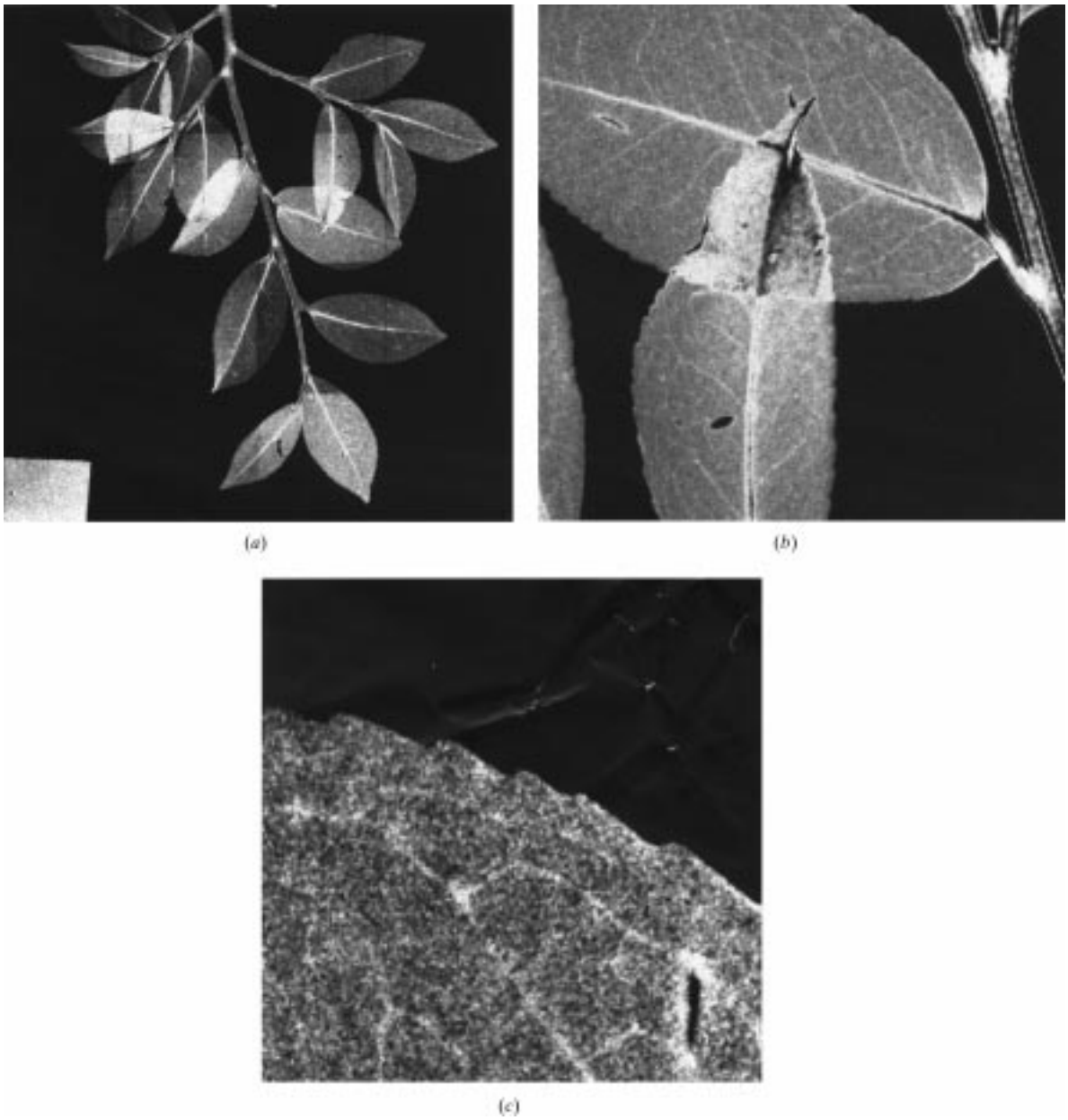

Figure 12
(*a*) An X-ray transmission image of a twig taken with the MCCDX. The actual size of the image is 200 mm × 200 mm. (*b*) An X-ray transmission image of a twig taken with a single CCD X-ray detector module. The actual size of the image is 50 mm × 50 mm. (*c*) A magnified X-ray transmission image of a leaf taken with the MCCDX. The actual size of the image is 17 mm × 17 mm.

The authors would like to express their gratitude to Dr A. P. Hammersley at ESRF who kindly permitted us to employ his 2D data-analysis program *FIT2D*.

References

Allinson, N. M. (1994). *J. Synchrotron Rad.* **1**, 54–62.

Ashton, J. E. U. (1993). *Third London Conference on Position-Sensitive Detectors*, 6–10 September 1993, Brunel University, UK.

Castelli, C. M., Allinson, N. M., Moon, K. J. & Watson, D. L. (1994). *Nucl. Instrum. Methods*, A**348**, 649–653.

Chappell, J. H. & Murray, S. S. (1984). *Nucl. Instrum. Methods*, **221**, 159–167.

Coleman, C. I. (1985). *Adv. Electron. Electron Phys.* **64***B*, 649–661.

Deckman, H. W. & Gruner, S. M. (1986). *Nucl. Instrum. Methods*, A**246**, 527–533.

EEV (1987). *CCD Imaging III.* EEV Ltd, Chelmsford, Essex CM1 2QU, UK.

EEV (1994*a*). *Large Area CCD Image Sensor CCD05-30 Series*, A1A-CCD05-30 Series Scientific Image Sensor Issue 3, January 1994. EEV Ltd, Chelmsford, Essex CM1 2QU, UK.

EEV (1994*b*). *CCD Driver Assembly CDB01-x User Manual*, CDB01-x Issue 1, April 1994. EEV Ltd, Chelmsford, Essex CM1 2QU, UK.

Eikenberry, E. F., Tate, M. W., Belmonte, A. L., Lowrance, J. L., Bilderback, D. & Gruner, S. M. (1991). *IEEE Trans. Nucl. Sci.* **38**, 110–118.

Flynt, W. E. (1989). *Proc. SPIE*, **1155**, 123–130.

Gruner, S. M., Barna, S. L., Wall, M. E., Tate, M. W. & Eikenberry, E. F. (1993). *Proc. SPIE*, **2009**, 98–108.

Hammersley, A. P., Brown, K., Burmeister, W., Claustre, L., Gonzalez, A., McSweeney, S., Mitchell, E., Moy, J.-P., Svensson, S. O. & Thompson, A. W. (1997). *J. Synchrotron Rad.* **4**, 67–77.

Hammersley, A. P., Svensson, S. O. & Thompson, A. (1994). *Nucl. Instrum. Methods*, A**346**, 312–321.

Hammersley, A. P., Svensson, S. O., Thompson, A., Graafsma, H., Kvick, Å. & Moy, J. P. (1995). *Rev. Sci. Instrum.* **66**(3), 2729–2733.

Helliwell, J. R. (1992). *Macromolecular Crystallography with Synchrotron Radiation*, pp. 181–211. Cambridge University Press.

Knoll, G. F. (1989). *Radiation Detection and Measurement*, 2nd ed., p. 231. New York: John Wiley and Sons.

Koch, A. (1994). *Nucl. Instrum. Methods*, A**348**, 654–658.

Moy, J. P. (1996). *Fibre Optics CCD Mosaic Area Detectors: a Survey of Commercial and Laboratory Systems.* ESRF Detector Group, ESRF, Grenoble, France.

Moy, J. P., Koch, A. & Nielsen, M. B. (1993). *Nucl. Instrum. Methods*, A**326**, 581–586.

Naday, I., Ross, S., Kanyo, M., Westbrook, E. & Westbrook, M. (1994). *Nucl. Instrum. Methods*, A**347**, 534–538.

Naday, I., Westbrook, E. M., Westbrook, M. L., Travis, D. J., Stanton, M., Phillips, W. C., O'Mara, D. & Xie, J. (1994). *Nucl. Instrum. Methods*, A**348**, 635–640.

O'Mara, D., Phillips, W., Stanton, M., Saroff, D., Naday, I. & Westbrook, E. M. (1992). *Proc. SPIE*, **1656**, 450–456.

Particle Data Group (1994). *Phys. Rev. D*, **50**, 1269.

Phillips, W., Stanton, M., O'Mara, D., Li, Y., Naday, I. & Westbrook, E. M. (1993). *Proc. SPIE*, **2009**, 133–138.

Shepherd, J. A., Gruner, S. M., Tate, M. W. & Tecotzky, M. (1997). *Opt. Eng.* **36**(11), 3212–3222.

Stanton, M. (1993). *Nucl. Instrum. Methods*, A**325**, 550–557.

Stanton, M. & Phillips, W. (1993). *Proc. SPIE*, **2009**, 128–132.

Stanton, M., Phillips, W. C., Li, Y. & Kalata, K. (1992*a*). *J. Appl. Cryst.* **25**, 549–558.

Stanton, M., Phillips, W. C., Li, Y. & Kalata, K. (1992*b*). *J. Appl. Cryst.* **25**, 638–645.

Stanton, M., Phillips, W. C., O'Mara, D., Naday, I. & Westbrook, E. (1993). *Nucl. Instrum. Methods*, A**325**, 558–567.

Strauss, M. G., Westbrook, E. M., Naday, I., Coleman, T. A., Westbrook, M. L., Travis, D. J., Sweet, R. M., Pflugrath, J. W. & Stanton, M. (1990). *Nucl. Instrum. Methods*, A**297**, 275–295.

Tate, M. W., Eikenberry, E. F., Barna, S. L., Wall, M. E., Lowrance, J. L. & Gruner, S. M. (1995). *J. Appl. Cryst.* **28**, 196–205.

Westbrook, E. M. & Naday, I. (1997). *Methods in Enzymology*, Vol. 276, edited by C. W. Carter & R. M. Sweet, pp. 244–268. New York: Academic Press.

Yamamoto, M., Kumasaka, T., Fujisawa, T. & Ueki, T. (1997). *J. Synchrotron Rad.* **5**, 222–225.